

Generative Model for Change Point Detection in Dynamic Graphs

Anonymous authors

Paper under double-blind review

Abstract

This paper proposes a generative model to detect change points in time series of graphs. The proposed framework consists of learnable prior distributions for low-dimensional graph representations and of a decoder that can generate graphs from the latent representations. The informative prior distributions in the latent spaces are learned from the observed data as empirical Bayes, and the expressive power of generative model is exploited to assist multiple change point detection. Specifically, the model parameters are learned via maximum approximate likelihood, with a Group Fused Lasso regularization on the prior parameters. The optimization problem is then solved via Alternating Direction Method of Multipliers (ADMM), and Langevin Dynamics are recruited for posterior inference. Experiments in both simulated and real data demonstrate the ability of the generative model in supporting change point detection with good performance.

1 Introduction

Networks are often used to represent relational phenomena in numerous domains (Dwivedi et al., 2021; He et al., 2023; Han et al., 2023), and relational phenomena by nature progress in time. In recent decades, a plethora of models has been proposed to analyze the interaction between objects or people over time, including Temporal Exponential-family Random Graph Model (Hanneke et al., 2010; Krivitsky & Handcock, 2014), Stochastic Actor-Oriented Model (Snijders, 2001; Snijders et al., 2010), and Relational Event Model (Butts, 2008; Butts et al., 2023). Though these models incorporate the temporal aspect for analysis, network evolution is usually time-heterogeneous. Without taking the structural changes across dynamic networks into consideration, learning from the time series may lead to ambiguity. Hence, it is practical for researchers to localize the change points in time, before studying the evolving networks.

Various methodologies have been proposed to detect change points in dynamic networks. Chen et al. (2020) employed embedding methods to detect both anomalous graphs and anomalous vertices in time series of networks. Park & Sohn (2020) combined the multi-linear tensor regression model with a hidden Markov model, detecting changes based on the transition between the hidden states. Sulem et al. (2023) learned a graph similarity function using a Siamese graph neural network to differentiate the graphs before and after a change point. Furthermore, Zhao et al. (2019) developed a screening algorithm that is based on an initial graphon estimation to detect change points. Huang et al. (2020) utilized the singular values of the Laplacian matrices as graph embedding to detect the differences across time. Chen & Zhang (2015), Chu & Chen (2019), and Song & Chen (2022a) proposed a non-parametric approach to delineate the distributional differences over time, and Garreau & Arlot (2018) and Song & Chen (2022b) exploited the patterns in high dimensions via a kernel-based method.

Inherently, network structures are complex due to highly dyadic dependency. Acquiring a low dimensional representation of the graph can summarize the enormous amount of individual relations to promote the downstream analysis. In particular, Sharifnia & Saghaei (2022) and Kei et al. (2023) proposed to detect the structural changes using an Exponential-family Random Graph Model. Yet they relied on user-specified network statistics, which are usually not known to the modeler a priori. Moreover, Larroca et al. (2021), Marenco et al. (2022), and Gong et al. (2023) developed different latent space models for dynamic graphs to

detect changes, but they focused on node level representation, which may not be powerful enough to capture the information of the entire graph. On the other hand, generative models recently showed promising results in myriad applications, such as text generation with Large Language Model (Devlin et al., 2018; Lewis et al., 2019) and image generation with Diffusion Model (Ho et al., 2020; Rombach et al., 2022). Likewise, we explore how generative models can assist change point detection for dynamic graphs.

To tackle these challenges, we make the following contributions in this manuscript:

- We learn graph level representations of network structures to facilitate change point detection. The informative prior distributions and a graph decoder are jointly learned via maximum approximate likelihood, with a multivariate total variation regularization.
- We derive an Alternating Direction Method of Multipliers (ADMM) procedure to solve the resulting optimization problem. The prior distributions and the graph decoder are learned by inferring from the posterior distribution via Langevin Dynamics. Experiments show good performance of the generative model in supporting change point detection.

The rest of the manuscript is organized as follows. Section 2 specifies the proposed framework. Section 3 presents the objective function with Group Fused Lasso regularization and the ADMM to solve the optimization problem. Section 4 discusses change points localization and model selection. Section 5 illustrates the proposed method on simulated and real data. Section 6 concludes the work with a discussion and potential future developments.

2 Generative Model for Change Point Detection

2.1 Model Specification

For a node set $N = \{1, 2, \dots, n\}$, we can use a network, graph, or adjacency matrix $\mathbf{y} \in \mathcal{Y}$ to represent the potential relations for all pairs $(i, j) \in \mathbb{Y} \subseteq N \times N$. The network \mathbf{y} has dyad $\mathbf{y}_{ij} \in \{0, 1\}$ to indicate the absence or presence of a relation between node i and node j , thence $\mathcal{Y} \subseteq 2^{\mathbb{Y}}$. The relations in a network can be either directed or undirected. The undirected variant has $\mathbf{y}_{ij} = \mathbf{y}_{ji}$ for all $(i, j) \in \mathbb{Y}$.

Denote $\mathbf{y}^t \in \mathcal{Y}^t \subseteq 2^{\mathbb{Y}}$ as a network at a discrete time point t . The observed data is a sequence of networks $\mathbf{y}^1, \dots, \mathbf{y}^T$. For each network \mathbf{y}^t , we assume there is a latent variable $\mathbf{z}^t \in \mathbb{R}^d$ such that the network \mathbf{y}^t can be generated from the latent variable with the following graph decoder:

$$\mathbf{y}^t \sim P(\mathbf{y}^t | \mathbf{z}^t) = \prod_{(i,j) \in \mathbb{Y}} \text{Bernoulli}(\mathbf{r}_{ij}(\mathbf{z}^t))$$

where $\mathbf{r}_{ij}(\mathbf{z}^t) = P(\mathbf{y}_{ij}^t = 1 | \mathbf{z}^t)$ is the Bernoulli parameter for dyad (i, j) and it is elaborated in Section 2.2. Conditioning on the latent variable \mathbf{z}^t , we assume the network \mathbf{y}^t is dyadic independent.

We also impose a learnable prior distribution to the latent variable as

$$\mathbf{z}^t \sim P(\mathbf{z}^t) = \mathcal{N}(\boldsymbol{\mu}^t, \mathbf{I}_d)$$

where $\boldsymbol{\mu}^t \in \mathbb{R}^d$ and \mathbf{I}_d is an identity matrix. With the graph decoder $P(\mathbf{y}^t | \mathbf{z}^t)$, we consider $\mathbf{z}^t \in \mathbb{R}^d$ as a graph level representation for $\mathbf{y}^t \in \{0, 1\}^{n \times n}$.

2.2 Graph Decoder

The graph decoder $P(\mathbf{y}^t | \mathbf{z}^t)$ is formulated with a Bernoulli parameter for dyad (i, j) as

$$\mathbf{r}_{ij}(\mathbf{z}^t) = P(\mathbf{y}_{ij}^t = 1 | \mathbf{z}^t) = \mathbf{g}_{ij}(\mathbf{h}(\mathbf{z}^t)).$$

The function $\mathbf{h}(\cdot)$ is parameterized by neural networks with $\mathbf{h} : \mathbb{R}^d \rightarrow \mathbb{R}^{n \times n}$. The function $\mathbf{g}(\cdot)$ is the element-wise sigmoid function with $\mathbf{g} : \mathbb{R}^{n \times n} \rightarrow [0, 1]^{n \times n}$.

In particular, we use multi-layer perceptrons, transferring the latent variable $\mathbf{z}^t \in \mathbb{R}^d$ to $\mathbf{U}^t \in \mathbb{R}^{n \times k}$ and $\mathbf{V}^t \in \mathbb{R}^{n \times k}$, respectively. We let the latent dimension d and k be smaller than the number of nodes n , and

$$\mathbf{h}(\mathbf{z}^t) = \begin{cases} \mathbf{U}^t \mathbf{V}^{t\top} \in \mathbb{R}^{n \times n}, & \text{for directed network,} \\ \mathbf{U}^t \mathbf{U}^{t\top} \in \mathbb{R}^{n \times n}, & \text{for undirected network.} \end{cases}$$

Figure 1 gives an overview of the proposed framework. Implicitly, the graph level representation \mathbf{z}^t progresses to node level representations \mathbf{U}^t and \mathbf{V}^t as an intermediate step, before the generation of network \mathbf{y}^t . The graph decoder $P_\phi(\mathbf{y}^t | \mathbf{z}^t)$ with neural network parameter ϕ is shared across $t = 1, \dots, T$. It is worth pointing out the simplicity of our framework, without the need of encoders.

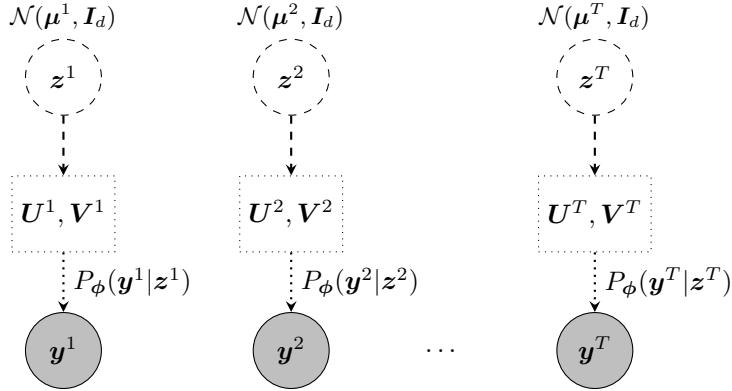


Figure 1: An overview of prior distributions and graph decoder.

2.3 Change Points

Anchored on the proposed framework, we can now specify the change points to be detected, in terms of the prior parameters $\boldsymbol{\mu}^t \in \mathbb{R}^d$ for $t = 1, \dots, T$. Let $\{C_k\}_{k=0}^{K+1} \subset \{1, 2, \dots, T\}$ be a collection of ordered change points with $1 = C_0 < C_1 < \dots < C_K < C_{K+1} = T$ such that

$$\begin{aligned} \boldsymbol{\mu}^{C_k} &= \boldsymbol{\mu}^{C_{k+1}} = \dots = \boldsymbol{\mu}^{C_{k+1}-1}, \quad k = 0, \dots, K, \\ \boldsymbol{\mu}^{C_k} &\neq \boldsymbol{\mu}^{C_{k+1}}, \quad k = 0, \dots, K-1, \quad \text{and} \quad \boldsymbol{\mu}^{C_{K+1}} = \boldsymbol{\mu}^{C_K}. \end{aligned}$$

The associated multiple change point detection problem comprises recovering the collection $\{C_k\}_{k=1}^K$ from a sequence of observed networks $\{\mathbf{y}^t\}_{t=1}^T$, where the number of change points K is also unknown. To facilitate change point detection for $\{\mathbf{y}^t\}_{t=1}^T$ in the data space, we turn to learn the prior parameters $\{\boldsymbol{\mu}^t\}_{t=1}^T$ in the latent space. Intuitively, the consecutive prior parameters are similar when no change occurs, but they are different when a change emerges. For notational simplicity, we denote $\boldsymbol{\mu} \in \mathbb{R}^{T \times d}$ as a matrix where the t -th row corresponds to $\boldsymbol{\mu}^t \in \mathbb{R}^d$ with $t = 1, \dots, T$.

3 Learning and Inference

3.1 Learning Priors from Dynamic Graphs

Inspired by Vert & Bleakley (2010) and Bleakley & Vert (2011), we formulate the change point detection problem as a Group Fused Lasso problem (Alaíz et al., 2013). Denote the log-likelihood of the model for $\mathbf{y}^1, \dots, \mathbf{y}^T$ as $l(\phi, \boldsymbol{\mu})$. We want to solve

$$\hat{\phi}, \hat{\boldsymbol{\mu}} = \arg \min_{\phi, \boldsymbol{\mu}} -l(\phi, \boldsymbol{\mu}) + \lambda \sum_{t=1}^{T-1} \|\boldsymbol{\mu}^{t+1} - \boldsymbol{\mu}^t\|_2 \quad (1)$$

where $\lambda > 0$ is a tuning parameter for the penalty term. Fundamentally, we impose the Group Fused Lasso penalty on the sequential differences of the prior parameters, so that the learned priors can incorporate the structural changes between consecutive graphs in the latent space. Specifically, we motivate the change point detection problem as a Group Fused Lasso problem because the regularization term, expressed as the sum of the ℓ_2 norms, encourages sparsity of the differences $\boldsymbol{\mu}^{t+1} - \boldsymbol{\mu}^t \in \mathbb{R}^d$, while allowing multiple coordinates across the d dimensional differences to change at the same time t . The latter is often referred as a grouping effect that could not be achieved with the ℓ_1 penalty of the differences. We refer the interested reader to the Figure 1 in Bleakley & Vert (2011) for a comparison.

To solve the optimization problem in (1) that involves latent variables, we need to manipulate the objective function accordingly. We first introduce a slack variable $\boldsymbol{\nu} \in \mathbb{R}^{T \times d}$ where $\boldsymbol{\nu}^t \in \mathbb{R}^d$ denotes the t -th row of matrix $\boldsymbol{\nu}$, and we can rewrite the original problem as a constrained optimization problem:

$$\begin{aligned} \hat{\boldsymbol{\phi}}, \hat{\boldsymbol{\mu}} = \arg \min_{\boldsymbol{\phi}, \boldsymbol{\mu}} & -l(\boldsymbol{\phi}, \boldsymbol{\mu}) + \lambda \sum_{t=1}^{T-1} \|\boldsymbol{\nu}^{t+1} - \boldsymbol{\nu}^t\|_2 \\ \text{subject to} & \boldsymbol{\mu} = \boldsymbol{\nu}. \end{aligned} \quad (2)$$

Then the augmented Lagrangian can be defined as

$$\mathcal{L}(\boldsymbol{\phi}, \boldsymbol{\mu}, \boldsymbol{\nu}, \boldsymbol{\rho}) = -l(\boldsymbol{\phi}, \boldsymbol{\mu}) + \lambda \sum_{t=1}^{T-1} \|\boldsymbol{\nu}^{t+1} - \boldsymbol{\nu}^t\|_2 + \text{tr}[\boldsymbol{\rho}^\top (\boldsymbol{\mu} - \boldsymbol{\nu})] + \frac{\kappa}{2} \|\boldsymbol{\mu} - \boldsymbol{\nu}\|_F^2$$

where $\boldsymbol{\rho} \in \mathbb{R}^{T \times d}$ is the Lagrange multipliers and $\kappa > 0$ is the penalty parameter for the augmentation term. Let $\boldsymbol{w} = \kappa^{-1} \boldsymbol{\rho} \in \mathbb{R}^{T \times d}$ be the scaled dual variable, the augmented Lagrangian can be updated to

$$\mathcal{L}(\boldsymbol{\phi}, \boldsymbol{\mu}, \boldsymbol{\nu}, \boldsymbol{w}) = -l(\boldsymbol{\phi}, \boldsymbol{\mu}) + \lambda \sum_{t=1}^{T-1} \|\boldsymbol{\nu}^{t+1} - \boldsymbol{\nu}^t\|_2 + \frac{\kappa}{2} \|\boldsymbol{\mu} - \boldsymbol{\nu} + \boldsymbol{w}\|_F^2 - \frac{\kappa}{2} \|\boldsymbol{w}\|_F^2. \quad (3)$$

In practice, gradient descent may not work well for an objective function with Group Fused Lasso penalty. We further introduce two variables $(\boldsymbol{\gamma}, \boldsymbol{\beta}) \in \mathbb{R}^{1 \times d} \times \mathbb{R}^{(T-1) \times d}$ to ease the optimization, by converting it into a Group Lasso problem (Yuan & Lin, 2006). They are defined as

$$\boldsymbol{\gamma} = \boldsymbol{\nu}^1 \quad \text{and} \quad \boldsymbol{\beta}_{t,\cdot} = \boldsymbol{\nu}^{t+1} - \boldsymbol{\nu}^t \quad \forall t = 1, \dots, T-1.$$

Reversely, the slack variable $\boldsymbol{\nu} \in \mathbb{R}^{T \times d}$ can be reconstructed as $\boldsymbol{\nu} = \mathbf{1}_{T,1} \boldsymbol{\gamma} + \mathbf{X} \boldsymbol{\beta}$, where \mathbf{X} is a $T \times (T-1)$ design matrix with $\mathbf{X}_{ij} = 1$ for $i > j$ and 0 otherwise. Substituting the $\boldsymbol{\nu}$ in (3) with $(\boldsymbol{\gamma}, \boldsymbol{\beta})$, we have

$$\mathcal{L}(\boldsymbol{\phi}, \boldsymbol{\mu}, \boldsymbol{\gamma}, \boldsymbol{\beta}, \boldsymbol{w}) = -l(\boldsymbol{\phi}, \boldsymbol{\mu}) + \lambda \sum_{t=1}^{T-1} \|\boldsymbol{\beta}_{t,\cdot}\|_2 + \frac{\kappa}{2} \|\boldsymbol{\mu} - \mathbf{1}_{T,1} \boldsymbol{\gamma} - \mathbf{X} \boldsymbol{\beta} + \boldsymbol{w}\|_F^2 - \frac{\kappa}{2} \|\boldsymbol{w}\|_F^2.$$

Thus, we can derive the following Alternating Direction Method of Multipliers (ADMM) algorithm to solve the constrained optimization problem in (2):

$$\boldsymbol{\phi}_{(a+1)}, \boldsymbol{\mu}_{(a+1)} = \arg \min_{\boldsymbol{\phi}, \boldsymbol{\mu}} -l(\boldsymbol{\phi}, \boldsymbol{\mu}) + \frac{\kappa}{2} \|\boldsymbol{\mu} - \boldsymbol{\nu}_{(a)} + \boldsymbol{w}_{(a)}\|_F^2, \quad (4)$$

$$\boldsymbol{\gamma}_{(a+1)}, \boldsymbol{\beta}_{(a+1)} = \arg \min_{\boldsymbol{\gamma}, \boldsymbol{\beta}} \lambda \sum_{t=1}^{T-1} \|\boldsymbol{\beta}_{t,\cdot}\|_2 + \frac{\kappa}{2} \|\boldsymbol{\mu}_{(a+1)} - \mathbf{1}_{T,1} \boldsymbol{\gamma} - \mathbf{X} \boldsymbol{\beta} + \boldsymbol{w}_{(a)}\|_F^2, \quad (5)$$

$$\boldsymbol{w}_{(a+1)} = \boldsymbol{\mu}_{(a+1)} - \boldsymbol{\nu}_{(a+1)} + \boldsymbol{w}_{(a)}, \quad (6)$$

where subscript a denotes the current ADMM iteration. We recursively implement the three updates until a convergence criterion is satisfied. Throughout the paper, details about the implementation are provided in Appendix 7.4.

3.2 Parameters Update

3.2.1 Updating μ and ϕ

In this section, we derive the updates for the prior and graph decoder parameters. Denote the objective function in (4) as $\mathcal{L}(\phi, \mu)$. Setting the gradients of $\mathcal{L}(\phi, \mu)$ with respect to the prior parameter $\mu^t \in \mathbb{R}^d$ to zeros, we have the following:

Proposition 1. *The solution for μ^t at an iteration of our proposed ADMM algorithm is a weighted sum:*

$$\mu^t = \frac{1}{1 + \kappa} \mathbb{E}_{P(\mathbf{z}^t | \mathbf{y}^t)}(\mathbf{z}^t) + \frac{\kappa}{1 + \kappa} (\boldsymbol{\nu}^t - \mathbf{w}^t) \quad (7)$$

between the conditional expectation of the latent variable under the posterior distribution $P(\mathbf{z}^t | \mathbf{y}^t)$ and the difference between the slack and the scaled dual variables. The term $\mathbf{w}^t \in \mathbb{R}^d$ denotes the t -th row of the scaled dual variable $\mathbf{w} \in \mathbb{R}^{T \times d}$. The derivation is provided in Appendix 7.1.

Moreover, the gradient of $\mathcal{L}(\phi, \mu)$ with respect to the graph decoder parameter ϕ is calculated as

$$\nabla_{\phi} \mathcal{L}(\phi, \mu) = - \sum_{t=1}^T \mathbb{E}_{P(\mathbf{z}^t | \mathbf{y}^t)} \left(\nabla_{\phi} \log P(\mathbf{y}^t | \mathbf{z}^t) \right). \quad (8)$$

The parameter ϕ can be updated efficiently through back-propagation.

Notably, calculating the solution in (7) and the gradient in (8) requires evaluating the conditional expectation under the posterior distribution $P(\mathbf{z}^t | \mathbf{y}^t) \propto P(\mathbf{y}^t | \mathbf{z}^t) \times P(\mathbf{z}^t)$. We employ Langevin Dynamics to sample from the posterior distribution, approximating the conditional expectations (Xie et al., 2017; 2018; Nijkamp et al., 2020; Pang et al., 2020). In particular, let subscript τ be the time step of the Langevin Dynamics and let δ be a small step size. Moving toward the gradient of the posterior with respect to the latent variable, the Langevin Dynamics to draw samples from the posterior distribution is achieved by iterating:

$$\begin{aligned} \mathbf{z}_{\tau+1}^t &= \mathbf{z}_{\tau}^t + \delta [\nabla_{\mathbf{z}^t} \log P(\mathbf{z}^t | \mathbf{y}^t)] + \sqrt{2\delta} \boldsymbol{\epsilon} \\ &= \mathbf{z}_{\tau}^t + \delta [\nabla_{\mathbf{z}^t} \log P_{\phi}(\mathbf{y}^t | \mathbf{z}^t) - (\mathbf{z}_{\tau}^t - \mu^t)] + \sqrt{2\delta} \boldsymbol{\epsilon} \end{aligned} \quad (9)$$

where $\boldsymbol{\epsilon} \sim \mathcal{N}(\mathbf{0}, \mathbf{I}_d)$ is a random perturbation to the process. The derivation is provided in Appendix 7.2.

3.2.2 Updating γ and β

In this section, we derive the update in (5), which is equivalent to solving a Group Lasso problem. In particular, we decompose the slack variable $\boldsymbol{\nu}$ to work with γ and β . With ADMM, the updates on γ and β do not require the observed network data $\{\mathbf{y}^t\}_{t=1}^T$.

By adapting the derivation in Bleakley & Vert (2011), we have the following for our proposed ADMM:

Proposition 2. *[Bleakley & Vert, 2011] The Group Lasso problem to update $\beta \in \mathbb{R}^{(T-1) \times d}$ is solved in a block coordinate descent manner, by iteratively applying the following equation to each row t :*

$$\beta_{t,\cdot} \leftarrow \frac{1}{\kappa \mathbf{X}_{\cdot,t}^{\top} \mathbf{X}_{\cdot,t}} \left(1 - \frac{\lambda}{\|\mathbf{b}_t\|_2} \right)_+ \mathbf{b}_t \quad (10)$$

where $(\cdot)_+ = \max(\cdot, 0)$ and

$$\mathbf{b}_t = \kappa \mathbf{X}_{\cdot,t}^{\top} (\boldsymbol{\mu}_{(a+1)} + \mathbf{w}_{(a)} - \mathbf{1}_{T,1} \gamma - \mathbf{X}_{\cdot,-t} \boldsymbol{\beta}_{-t,\cdot}).$$

The derivation is provided in Appendix 7.3.

The convergence of the procedure can be monitored by the Karush-Kuhn-Tucker conditions: for all $\beta_{t,\cdot} \neq \mathbf{0}$,

$$\lambda \frac{\beta_{t,\cdot}}{\|\beta_{t,\cdot}\|_2} - \kappa \mathbf{X}_{\cdot,t}^{\top} (\boldsymbol{\mu}_{(a+1)} + \mathbf{w}_{(a)} - \mathbf{1}_{T,1} \gamma - \mathbf{X} \boldsymbol{\beta}) = \mathbf{0},$$

and for all $\beta_{t,\cdot} = \mathbf{0}$,

$$\|-\kappa \mathbf{X}_{\cdot,t}^\top (\boldsymbol{\mu}_{(a+1)} + \mathbf{w}_{(a)} - \mathbf{1}_{T,1} \boldsymbol{\gamma} - \mathbf{X} \boldsymbol{\beta})\|_2 \leq \lambda.$$

Lastly, for any $\boldsymbol{\beta}$, the minimum in $\boldsymbol{\gamma} \in \mathbb{R}^{1 \times d}$ is achieved at

$$\boldsymbol{\gamma} = (1/T) \mathbf{1}_{1,T} \cdot (\boldsymbol{\mu}_{(a+1)} + \mathbf{w}_{(a)} - \mathbf{X} \boldsymbol{\beta}).$$

In summary, the algorithm to solve the problem in (2) via ADMM is presented in Algorithm 1. The steps to transform between $\boldsymbol{\nu}$ and $(\boldsymbol{\gamma}, \boldsymbol{\beta})$ within an ADMM iteration are omitted for succinctness.

Algorithm 1 Latent Space Group Fused Lasso

- 1: **Input:** learning iterations A, B, D , tuning parameter λ , penalty parameter κ , learning rates η , observed data $\{\mathbf{y}^t\}_{t=1}^T$, initialization $\{\boldsymbol{\phi}_{(1)}, \boldsymbol{\mu}_{(1)}, \boldsymbol{\gamma}_{(1)}, \boldsymbol{\beta}_{(1)}, \mathbf{w}_{(1)}\}$
 - 2: **for** $a = 1, \dots, A$ **do**
 - 3: **for** $t = 1, \dots, T$ **do**
 - 4: draw s samples $\mathbf{z}_1^t, \dots, \mathbf{z}_s^t$ from $P(\mathbf{z}^t | \mathbf{y}^t)$ according to (9)
 - 5: $\boldsymbol{\mu}_{(a+1)}^t = \frac{1}{1+\kappa} (s^{-1} \sum_{i=1}^s \mathbf{z}_i^t) + \frac{\kappa}{1+\kappa} (\boldsymbol{\nu}^t - \mathbf{w}^t)$
 - 6: **end for**
 - 7: **for** $b = 1, \dots, B$ **do**
 - 8: $\boldsymbol{\phi}_{(b+1)} = \boldsymbol{\phi}_{(b)} - \eta \times \nabla_{\boldsymbol{\phi}} \mathcal{L}(\boldsymbol{\phi}, \boldsymbol{\mu})$
 - 9: **end for**
 - 10: Set $\tilde{\boldsymbol{\gamma}}^{(1)} = \boldsymbol{\gamma}_{(a)}, \tilde{\boldsymbol{\beta}}^{(1)} = \boldsymbol{\beta}_{(a)}$
 - 11: **for** $d = 1, \dots, D$ **do**
 - 12: **for** $t = 1, \dots, T-1$ **do**
 - 13: Let $\tilde{\boldsymbol{\beta}}_{t,\cdot}^{(d+1)}$ be updated according to (10)
 - 14: **end for**
 - 15: $\tilde{\boldsymbol{\gamma}}^{(d+1)} = (1/T) \mathbf{1}_{1,T} \cdot (\boldsymbol{\mu}_{(a+1)} + \mathbf{w}_{(a)} - \mathbf{X} \tilde{\boldsymbol{\beta}}^{(d+1)})$
 - 16: **end for**
 - 17: Set $\boldsymbol{\gamma}_{(a+1)} = \tilde{\boldsymbol{\gamma}}^{(d+1)}, \boldsymbol{\beta}_{(a+1)} = \tilde{\boldsymbol{\beta}}^{(d+1)}$
 - 18: $\mathbf{w}_{(a+1)} = \boldsymbol{\mu}_{(a+1)} - \boldsymbol{\nu}_{(a+1)} + \mathbf{w}_{(a)}$
 - 19: **end for**
 - 20: $\hat{\boldsymbol{\mu}} \leftarrow \boldsymbol{\mu}_{(a+1)}$
 - 21: **Output:** learned prior parameters $\hat{\boldsymbol{\mu}}$
-

4 Change Point Localization and Model Selection

4.1 Change Point Localization

In this section, we provide two effective methods to localize the change points after parameter learning, and they can be used for different purposes. For the first approach, we can resort to the prior distribution where $\mathbf{z}^t \sim \mathcal{N}(\boldsymbol{\mu}^t, \mathbf{I}_d)$. When no change occurs or $\boldsymbol{\mu}^t - \boldsymbol{\mu}^{t-1} = \mathbf{0}$, we have $\mathbf{z}^t - \mathbf{z}^{t-1} \sim \mathcal{N}(\mathbf{0}, 2\mathbf{I}_d)$ and

$$u^t := \frac{1}{2} (\mathbf{z}^t - \mathbf{z}^{t-1})^\top (\mathbf{z}^t - \mathbf{z}^{t-1}) \sim \chi_d^2.$$

Furthermore, the mean of u^t over m samples follows a Gamma distribution:

$$\bar{u}^t \sim \Gamma(\theta = \frac{2}{m}, \xi = \frac{md}{2})$$

where θ and ξ are the respective scale and shape parameters.

As we capture the structural changes in the latent space, we can draw samples from the learned priors to reflect the sequential changes. In particular, for a time point t , we sample $\hat{\mathbf{z}}^t - \hat{\mathbf{z}}^{t-1}$ from $\mathcal{N}(\hat{\boldsymbol{\mu}}^t - \hat{\boldsymbol{\mu}}^{t-1}, 2\mathbf{I}_d)$, and we perform the same transformation:

$$v^t := \frac{1}{2} (\hat{\mathbf{z}}^t - \hat{\mathbf{z}}^{t-1})^\top (\hat{\mathbf{z}}^t - \hat{\mathbf{z}}^{t-1}).$$

Then we compare the mean of v^t over m samples with a quantile:

$$P(\bar{v}^t > q_{\text{thr}}) = 1 - \frac{\alpha}{T-1} \quad (11)$$

where q_{thr} is the $1 - \alpha/(T-1)$ quantile of the Gamma distribution for \bar{u}^t when no change occurs. We consider the time point t with $\bar{v}^t > q_{\text{thr}}$ as the detected change point.

For the second approach, we can utilize the localizing method from Kei et al. (2023), which is more robust in practice, as compared in the simulation study of Section 5.1. First, we calculate the differences between consecutive time points in $\hat{\boldsymbol{\mu}} \in \mathbb{R}^{T \times d}$ as

$$\Delta \hat{\boldsymbol{\mu}}^t = \|\boldsymbol{\mu}^t - \boldsymbol{\mu}^{t-1}\|_2 \quad \forall t \in [2, T].$$

Then we standardize the differences as

$$\Delta \hat{\boldsymbol{\zeta}}^t = \frac{\Delta \hat{\boldsymbol{\mu}}^t - \text{median}(\Delta \hat{\boldsymbol{\mu}})}{\text{std}(\Delta \hat{\boldsymbol{\mu}})} \quad \forall t \in [2, T] \quad (12)$$

and construct a data-driven threshold defined as

$$\mathcal{T}_{\text{thr}} := \text{mean}(\Delta \hat{\boldsymbol{\zeta}}) + \mathcal{Z}_q \times \text{sd}(\Delta \hat{\boldsymbol{\zeta}}) \quad (13)$$

where \mathcal{Z}_q is the $q\%$ quantile of standard Normal distribution. Finally, we declare a change point C_k when $\Delta \hat{\boldsymbol{\zeta}}^{C_k} > \mathcal{T}_{\text{thr}}$.

The data-driven threshold in (13) is intuitive, as the standardized differences $\Delta \hat{\boldsymbol{\zeta}}$ between two consecutive change points are close to zeros, while the differences that are at the change points are substantially greater than zeros. When traced in a plot over time t , the $\Delta \hat{\boldsymbol{\zeta}}$ can exhibit the magnitude of structural changes, and the threshold that deviates from the mean provides a reasonable cut-off value for the standardized differences, as demonstrated in Figures 5 and 6. In summary, the localizing method derived from the prior distribution has a statistical justification, while the localizing method with the data-driven threshold is more robust for different types of network data in practice.

4.2 Model Selection

The optimization problem in (2) involves a tuning parameter that can yield different sets of detected change points when it is varied. In this work, we use Cross-Validation to select λ . In particular, we split the original time series of graphs into training and testing sets: the training set consists of graphs at odd indexed time points and the testing set consists of graphs at even indexed time points. Fixed on a specific λ value, we learn the model parameters with the training set, and we evaluate the learned model with the testing set.

For a list of λ values, we choose the λ giving the maximal log-likelihood on the testing set. Note that the log-likelihood is approximated by Monte Carlo samples $\{\mathbf{z}_u^t\}_{u=1}^s$ drawn from the prior distribution $P(\mathbf{z}^t)$ as

$$\sum_{t=1}^T \log P(\mathbf{y}^t) \approx \sum_{t=1}^T \log \left[\frac{1}{s} \sum_{u=1}^s \left[\prod_{(i,j) \in \mathcal{Y}} P_{\phi}(\mathbf{y}_{ij}^t | \mathbf{z}_u^t) \right] \right].$$

Further computational details are discussed in Appendix 7.4. Anchored on the selected λ value, we learn the model parameters again with the full data, resulting the final set of detected change points.

5 Simulated and Real Data Experiments

In this section, we implement the proposed method on simulated and real data. To evaluate the performance for simulated data, we use three standard metrics in the literature that focus on the number of change points, the time gap between the true and detected change points, and the coverage between the segmented time intervals. The first metric is the absolute error $|\hat{K} - K|$, where \hat{K} and K are the respective numbers of

the detected and true change points. The second metric described in Madrid Padilla et al. (2021) is the one-sided Hausdorff distance, which is defined as

$$d(\hat{\mathcal{C}}|\mathcal{C}) = \max_{c \in \mathcal{C}} \min_{\hat{c} \in \hat{\mathcal{C}}} |\hat{c} - c|$$

where $\hat{\mathcal{C}}$ and \mathcal{C} are the respective sets of detected and true change points. Also, we report the reversed one-sided Hausdorff distance $d(\mathcal{C}|\hat{\mathcal{C}})$. By convention, when $\hat{\mathcal{C}} = \emptyset$, we let $d(\hat{\mathcal{C}}|\mathcal{C}) = \infty$ and $d(\mathcal{C}|\hat{\mathcal{C}}) = -\infty$. The last metric described in van den Burg & Williams (2020) is the coverage of a partition \mathcal{G} by another partition \mathcal{G}' , which is defined as

$$C(\mathcal{G}, \mathcal{G}') = \frac{1}{T} \sum_{\mathcal{A} \in \mathcal{G}} |\mathcal{A}| \cdot \max_{\mathcal{A}' \in \mathcal{G}'} \frac{|\mathcal{A} \cap \mathcal{A}'|}{|\mathcal{A} \cup \mathcal{A}'|}$$

with $\mathcal{A}, \mathcal{A}' \subseteq [1, T]$. The \mathcal{G} and \mathcal{G}' are collections of intervals between consecutive change points for the respective true and detected change points.

5.1 Simulation Study

We simulate dynamic graphs from three scenarios to compare the performance of the proposed and competing methods: Separable Temporal Exponential Random Graph Model, Stochastic Block Model, and Recurrent Neural Network. For each scenario with different numbers of nodes $n \in \{50, 100\}$, we simulate 10 Monte Carlo trials of directed dynamic graphs with time span $T = 100$. The true change points are located at $t = 26, 51, 76$, so the number of change points $K = 3$. Moreover, the $K + 1 = 4$ intervals in the partition \mathcal{G} are $\mathcal{A}_1 = [1, \dots, 25]$, $\mathcal{A}_2 = [26, \dots, 50]$, $\mathcal{A}_3 = [51, \dots, 75]$, and $\mathcal{A}_4 = [76, \dots, 100]$. In each specification, we report the means and standard deviations over 10 Monte Carlo trials for the evaluation metrics. CPDlatent_N denotes our proposed approach with the data-driven threshold in (13), using 90% quantile from standard Normal distribution. We let the latent dimensions $d = 10$ and $k = 5$ for the graph decoder. CPDlatent_G denotes our proposed approach with the localizing method in (11), using $\alpha = 0.01$ from Gamma distribution. We let the latent dimensions $k = 10$ and $d = n/10$ for the graph decoder. The number of samples drawn from the Gamma distribution is $m = 500$ when $d = 10$ and $m = 1000$ when $d = 5$.

Three competitors, gSeg (Chen & Zhang, 2015), kerSeg (Song & Chen, 2022b), and CPDstergm (Kei et al., 2023), are provided for comparison. The gSeg utilizes graph-based scan statistics and kerSeg employs a kernel-based framework to test the partition before and after a change point. The CPDstergm fits a STERGM with user-specified network statistics to detect change points based on the model parameters. For CPDstergm, we first use two network statistics, edge count and mutuality, in both formation and dissolution models to let $p = 4$. We then add one more network statistic, number of triangles, to let $p = 6$ as another specification. For gSeg, we use the minimum spanning tree to construct the similarity graph, with the approximated p-value of the original edge-count scan statistic, and we set $\alpha = 0.05$. For kerSeg, we use the approximated p-value of the fGKCP₁, and we set $\alpha = 0.001$. Moreover, we use networks (nets.) and network statistics (stats.) as two types of input data to gSeg and kerSeg. Throughout, we choose these settings because they produce good performance on average for the competitors. Changing the settings can enhance their performance on some specifications, while severely jeopardizing their performance on other specifications.

Scenario 1: Separable Temporal Exponential Random Graph Model

In this scenario, we apply time-homogeneous Separable Temporal Exponential Random Graph Model (STERGM) between change points to generate sequences of dynamic networks (Krivitsky & Handcock, 2014). We use three network statistics, edge count, mutuality, and number of triangles, in both formation (F) and dissolution (D) models. The $p = 6$ parameters for each time point t are

$$\theta_F^t, \theta_D^t = \begin{cases} -2, 2, -2, -1, 2, 1, & t \in \mathcal{A}_1 \cup \mathcal{A}_3 \setminus 1, \\ -1.5, 1, -1, 2, 1, 1.5, & t \in \mathcal{A}_2 \cup \mathcal{A}_4. \end{cases}$$

Figure 2 exhibits examples of generated networks. Visually, STERGM produces adjacency matrices that are sparse, which is often the case in real world social networks.

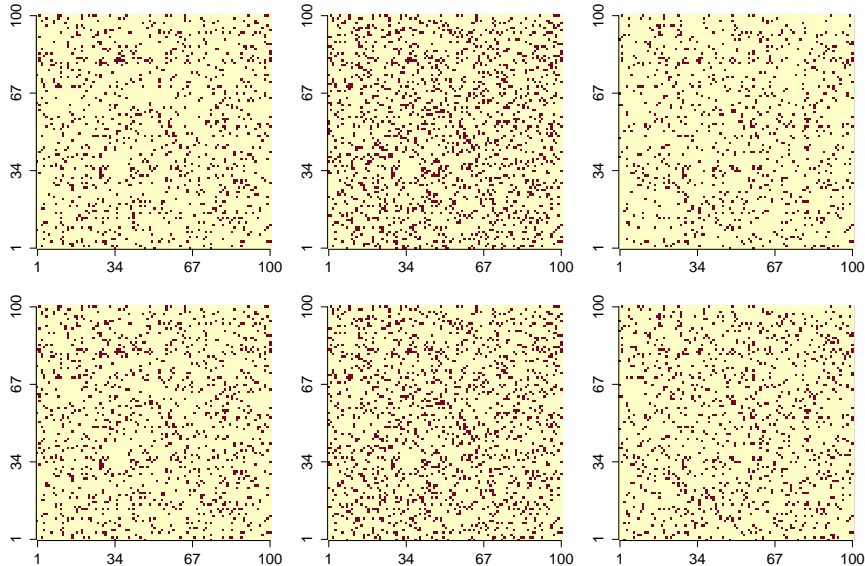


Figure 2: Examples of networks generated from STERGM with $n = 100$. In the first row, from left to right, each plot corresponds to the network at $t = 25, 50, 75$ respectively. In the second row, from left to right, each plot corresponds to the network at $t = 26, 51, 76$ respectively (the change points).

Tables 1 displays the means and standard deviations of the evaluation metrics for comparison. Since the networks are directly sampled from STERGM, the CPDstergm method with correctly specified network statistics ($p = 6$) achieves the best result, in terms of greater converge of the intervals. However, when the network statistics are mis-specified ($p = 4$), the performance of CPDstergm is worsened, with greater gaps between the true and detected change points. Also, using either networks (nets.) or network statistics (stats.) cannot improve the performance of gSeg and kerSeg methods: the binary search approach tend to detect excessive number of change points. Our CPDlatent method, without the need of specifying network statistics, can achieve relatively good performance on average.

Scenario 2: Stochastic Block Model

In this scenario, we use Stochastic Block Model (SBM) to generate sequences of dynamic networks, and we impose a time-dependent mechanism in the generation process as in Madrid Padilla et al. (2022). Two probability matrices $\mathbf{P}, \mathbf{Q} \in [0, 1]^{n \times n}$ are constructed and they are defined as

$$\mathbf{P}_{ij} = \begin{cases} 0.5, & i, j \in \mathcal{B}_l, l \in [3], \\ 0.3, & \text{otherwise,} \end{cases} \quad \text{and} \quad \mathbf{Q}_{ij} = \begin{cases} 0.45, & i, j \in \mathcal{B}_l, l \in [3], \\ 0.2, & \text{otherwise,} \end{cases}$$

where $\mathcal{B}_1, \mathcal{B}_2, \mathcal{B}_3$ are evenly sized clusters that form a partition of $\{1, \dots, n\}$. Then a sequence of matrices $\mathbf{E}^t \in [0, 1]^{n \times n}$ are arranged for $t = 1, \dots, T$ such that

$$\mathbf{E}_{ij}^t = \begin{cases} \mathbf{P}_{ij}, & t \in \mathcal{A}_1 \cup \mathcal{A}_3, \\ \mathbf{Q}_{ij}, & t \in \mathcal{A}_2 \cup \mathcal{A}_4. \end{cases}$$

Lastly, the networks are generated with $\rho = 0.5$ as a time-dependent mechanism. For $t = 1, \dots, T - 1$, we let $\mathbf{y}_{ij}^1 \sim \text{Bernoulli}(\mathbf{E}_{ij}^1)$ and

$$\mathbf{y}_{ij}^{t+1} \sim \begin{cases} \text{Bernoulli}(\rho(1 - \mathbf{E}_{ij}^{t+1}) + \mathbf{E}_{ij}^{t+1}), & \mathbf{y}_{ij}^t = 1, \\ \text{Bernoulli}((1 - \rho)\mathbf{E}_{ij}^{t+1}), & \mathbf{y}_{ij}^t = 0. \end{cases}$$

Table 1: Means (standard deviations) of evaluation metrics for dynamic graphs simulated from STERGM. The best coverage metric is bolded.

n	Method	$ \hat{K} - K \downarrow$	$d(\hat{\mathcal{C}} \mathcal{C}) \downarrow$	$d(\mathcal{C} \hat{\mathcal{C}}) \downarrow$	$C(\mathcal{G}, \mathcal{G}') \uparrow$
50	CPDlatent $_N$	0.1 (0.3)	4.3 (5.7)	2.6 (1.3)	90.87%
	CPDlatent $_G$	0.4 (0.6)	4.2 (6.9)	3.4 (3.4)	90.97%
	CPDstergm $_{p=4}$	1.5 (0.8)	11.7 (7.5)	10.5 (2.3)	67.68%
	CPDstergm $_{p=6}$	0.2 (0.4)	1.6 (1.2)	3 (3.5)	91.54%
	gSeg (nets.)	12.3 (0.5)	0 (0)	19 (0)	27.90%
	gSeg (stats.)	15.8 (0.7)	1.5 (0.5)	20.1 (0.3)	24.55%
	kerSeg (nets.)	9.7 (0.9)	1.4 (0.9)	17.9 (1.2)	37.62%
	kerSeg (stats.)	9.4 (0.7)	3.9 (1.3)	18 (1.8)	35.86%
100	CPDlatent $_N$	0 (0)	3.9 (1.3)	3.9 (1.3)	91.33%
	CPDlatent $_G$	0.7 (1.3)	3.1 (1.3)	6.0 (4.0)	88.55%
	CPDstergm $_{p=4}$	0.7 (0.6)	21.9 (10.3)	7.6 (4.3)	67.21%
	CPDstergm $_{p=6}$	0 (0)	1.1 (0.3)	1.1 (0.3)	94.01%
	gSeg (nets.)	12 (0)	0 (0)	19 (0)	28.00%
	gSeg (stats.)	14.5 (2.3)	3.3 (3.6)	20.2 (0.4)	26.13%
	kerSeg (nets.)	9.3 (0.8)	1 (0)	17.7 (0.6)	37.62%
	kerSeg (stats.)	8.5 (0.8)	4.5 (1.4)	17.3 (1.7)	36.92%

With $\rho > 0$, the probability to form an edge for i, j becomes greater at time $t + 1$ when there exists an edge at time t , and the probability becomes smaller when there does not exist an edge at time t . Figure 3 exhibits examples of generated networks. Visually, SBM produces adjacency matrices with block structures, where mutuality serves as an important pattern for the homophily within groups.

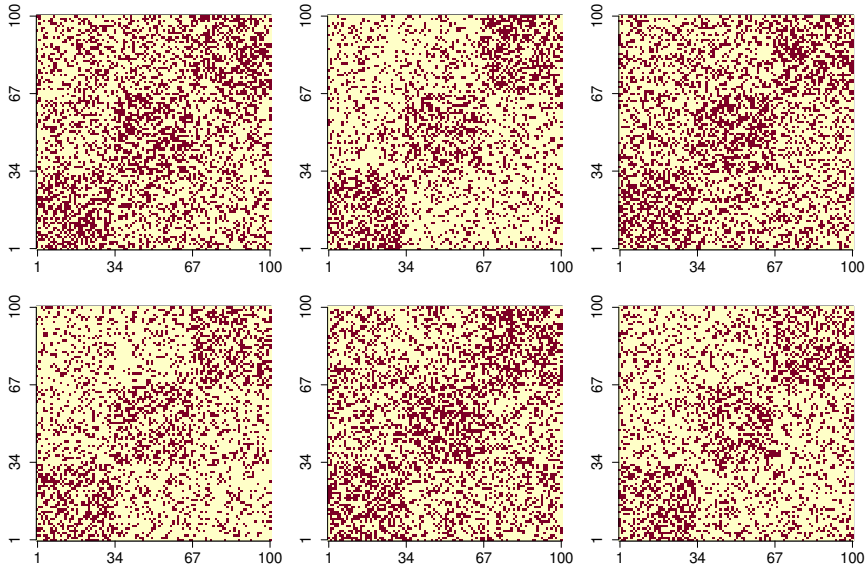


Figure 3: Examples of networks generated from SBM with $n = 100$. In the first row, from left to right, each plot corresponds to the network at $t = 25, 50, 75$ respectively. In the second row, from left to right, each plot corresponds to the network at $t = 26, 51, 76$ respectively (the change points).

Table 2: Means (stds.) of evaluation metrics for dynamic networks simulated from SBM. The best coverage metric is bolded.

n	Method	$ \hat{K} - K \downarrow$	$d(\hat{\mathcal{C}} \mathcal{C}) \downarrow$	$d(\mathcal{C} \hat{\mathcal{C}}) \downarrow$	$C(\mathcal{G}, \mathcal{G}') \uparrow$
50	CPDlatent $_N$	0 (0)	0.1 (0.3)	0.1 (0.3)	99.80%
	CPDlatent $_G$	0.3 (0.6)	0.1 (0.3)	3.1 (6.2)	96.70%
	CPDstergm $_{p=4}$	0.1 (0.3)	1 (0)	2.4 (4.2)	97.04%
	CPDstergm $_{p=6}$	0.3 (0.5)	1 (0)	4.6 (5.6)	94.74%
	gSeg (nets.)	12.9 (1.8)	0 (0)	19.4 (0.8)	27.20%
	gSeg (stats.)	2.2 (0.7)	Inf (na)	-Inf (na)	49.21%
	kerSeg (nets.)	6.4 (1.4)	0 (0)	16.6 (2.0)	45.50%
	kerSeg (stats.)	0.9 (1.2)	0 (0)	5.6 (6.8)	93.50%
100	CPDlatent $_N$	0.1 (0.3)	0.1 (0.3)	1.3 (3.6)	98.60%
	CPDlatent $_G$	0.5 (0.7)	0.2 (0.4)	5.1 (6.1)	94.81%
	CPDstergm $_{p=4}$	0 (0)	1 (0)	1 (0)	98.04%
	CPDstergm $_{p=6}$	0 (0)	1 (0)	1 (0)	98.04%
	gSeg (nets.)	12.3 (0.9)	0 (0)	19 (0)	27.80%
	gSeg (stats.)	2 (0.4)	Inf (na)	-Inf (na)	55.75%
	kerSeg (nets.)	6 (0.8)	0 (0)	15.2 (2.0)	47.00%
	kerSeg (stats.)	0.9 (0.7)	0 (0)	9.6 (7.6)	93.40%

Tables 2 displays the means and standard deviations of the evaluation metrics for comparison. As expected, both CPDstergm methods with $p = 4$ and $p = 6$ that utilize the mutuality as a sufficient statistic for the detection can achieve good results, in terms of greater converge of the intervals. Furthermore, using network statistics (stats.) for both gSeg and kerSeg methods can improve their performance, comparing to using networks (nets.) as input data. Lastly, our CPDlatent method, which infers the features in latent space that induce the structural changes, achieves the best result for networks with block structures.

Scenario 3: Recurrent Neural Networks

In this scenario, we use Recurrent Neural Networks (RNN) to generate sequences of dynamic networks. Specifically, we sample latent variables from pre-defined priors, and we initialize the RNN with uniform weights. The graphs are then generated by the matrix multiplication defined in Section 2.2, using the output of RNN. The parameters for the pre-defined priors are

$$\mathbf{z}^t \sim \begin{cases} \mathcal{N}(-\mathbf{1}, 0.1\mathbf{I}_d), & t \in \mathcal{A}_1 \cup \mathcal{A}_3, \\ \mathcal{N}(\mathbf{5}, 0.1\mathbf{I}_d), & t \in \mathcal{A}_2 \cup \mathcal{A}_4. \end{cases}$$

Similar to the previous two scenarios, the simulation using RNN also imposes a time-dependent mechanism across dynamic networks. Figure 5.1 exhibits examples of generated networks. Visually, RNN produces adjacency matrices that are dense, and no discernible pattern can be noticed.

Tables 3 displays the means and standard deviations of the evaluation metrics for comparison. Because no structural pattern or suitable network statistics can be determined a priori, neither CPDstergm method with $p = 4$ nor with $p = 6$ can detect the change points accurately. Likewise, both gSeg and kerSeg methods that utilize the mis-specified network statistics (stats.) cannot produce satisfactory performance. Notably, the kerSeg method that exploits the features in high dimension with networks (nets.) instead of user-specified network statistics (stats.) can deliver a good result. Lastly, our CPDlatent method that first infers the graph level representations from the complex network structures and then utilize them to detect the change points yields the best result.

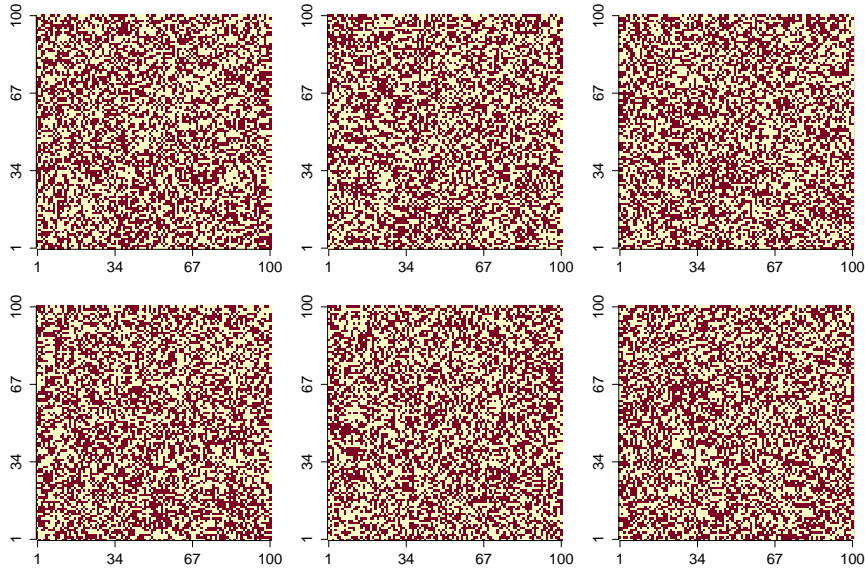


Figure 4: Examples of networks generated from RNN with $n = 100$. In the first row, from left to right, each plot corresponds to the network at $t = 25, 50, 75$ respectively. In the second row, from left to right, each plot corresponds to the network at $t = 26, 51, 76$ respectively (the change points).

Table 3: Means (stds.) of evaluation metrics for dynamic networks simulated from RNN. The best coverage metric is bolded.

n	Method	$ \hat{K} - K \downarrow$	$d(\hat{\mathcal{C}} \mathcal{C}) \downarrow$	$d(\mathcal{C} \hat{\mathcal{C}}) \downarrow$	$C(\mathcal{G}, \mathcal{G}') \uparrow$
50	CPDlatent $_N$	0 (0)	1.8 (0.7)	1.8 (0.7)	94.77%
	CPDlatent $_G$	0.3 (0.6)	1.7 (0.6)	3.2 (3.0)	93.04%
	CPDstergm $_{p=4}$	2.0 (1.7)	6.0 (7.7)	15.2 (4.9)	72.10%
	CPDstergm $_{p=6}$	1.0 (0.4)	18.5 (9.4)	14.3 (2.9)	60.25%
	gSeg (nets.)	2.3 (0.6)	Inf (na)	-Inf (na)	29.42%
	gSeg (stats.)	2.9 (0.3)	Inf (na)	-Inf (na)	2.47%
	kerSeg (nets.)	1.5 (0.9)	1.4 (0.7)	5.3 (3.3)	89.25%
	kerSeg (stats.)	2.8 (0.4)	Inf (na)	-Inf (na)	9.89%
100	CPDlatent $_N$	0 (0)	2.5 (0.7)	2.5 (0.7)	91.96%
	CPDlatent $_G$	0.2 (0.6)	2.1 (0.7)	2.8 (1.8)	92.34%
	CPDstergm $_{p=4}$	2.0 (1.4)	10.6 (8.0)	14.1 (3.1)	60.37%
	CPDstergm $_{p=6}$	1.2 (1.3)	20.6 (12.6)	15.2 (5.9)	53.21%
	gSeg (nets.)	3 (0)	Inf (na)	-Inf (na)	0%
	gSeg (stats.)	2.9 (0.3)	Inf (na)	-Inf (na)	4.27%
	kerSeg (nets.)	1.4 (0.7)	1.9 (0.7)	5.4 (1.9)	88.95%
	kerSeg (stats.)	3 (0)	Inf (na)	-Inf (na)	0%

5.2 MIT Cellphone Data

The Massachusetts Institute of Technology (MIT) cellphone data (Eagle & Pentland, 2006) depicts human interactions via phone call activities among $n = 96$ participants spanning $T = 232$ days. An edge $\mathbf{y}_{ij}^t = 1$ in

the constructed networks indicates that participant i and participant j had made phone calls on day t , and $y_{ij}^t = 0$ otherwise. The data ranges from 2004-09-15 to 2005-05-04, covering the winter break in the MIT academic calendar.

We detect the change points with our proposed method using the data-driven threshold from standard Normal distribution, and we use network statistics as input data to the competitor methods. Specifically, we use the number of edges, isolates, and triangles to capture the frequency of connections, the sparsity of social interaction, and the transitive association among friends, respectively. Figure 5 displays $\Delta\hat{\zeta}$ of Equation (12), and the detected change points from our method and competitor methods. Furthermore, Table 4 provides a list of potential events, aligning with the detected change points from our method.

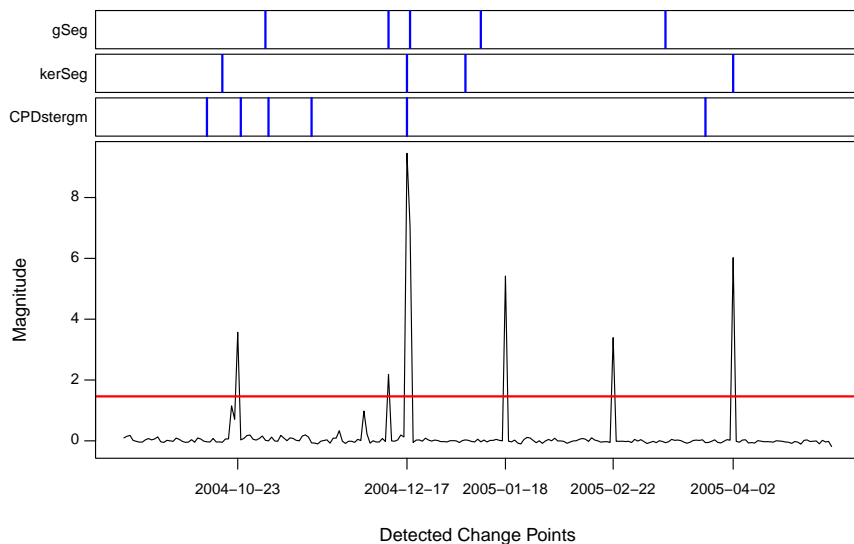


Figure 5: Detected change points from the proposed and competitor (blue) methods on the MIT Cellphone Data. The threshold (red horizontal line) is calculated by (13) with $\mathcal{Z}_{0.9}$.

Without specifying the structural changes to search for, our method can punctually detect the beginning of the winter break, which is the major event that alters the interaction among participants. Similar to the competitors, we have detected a spike on 2004-10-23, corresponding to the annual sponsor meeting that occurred on 2004-10-21. More than two-thirds of the participants have attended the meeting, focusing on achieving project goals throughout the week (Eagle & Pentland, 2006). Moreover, we have detected other change points related to national holidays and spring break.

Table 4: Potential nearby events aligned with the detected change points from our proposed method on the MIT cellphone data.

Detected change points	Potential nearby events
2004-10-23	2004-10-21 Sponsor meeting
2004-12-17	2004-12-18 to 2005-01-02 Winter break
2005-01-18	2005-01-17 Martin Luther King Day
2005-02-22	2005-02-21 Presidents Day
2005-04-02	2005-03-21 to 2005-03-25 Spring break

5.3 Enron Email Data

The Enron email data, analyzed by (Priebe et al., 2005; Park et al., 2012; Peel & Clauset, 2015), portrays communication among employees before the collapse of a giant energy company. The dynamic network data consists of $T = 100$ weekly networks, ranging from 2000-06-05 to 2002-05-06 for $n = 100$ employees. We detect the change points with our proposed method using the data-driven threshold from standard Normal distribution, and we use the same network statistics described in Section 5.2 to the competitor methods. Figure 6 displays $\Delta\hat{\zeta}$ of Equation (12), and the detected change points from our method and competitor methods. Furthermore, Table 5 provides a list of potential events, aligning with the detected change points from our method.

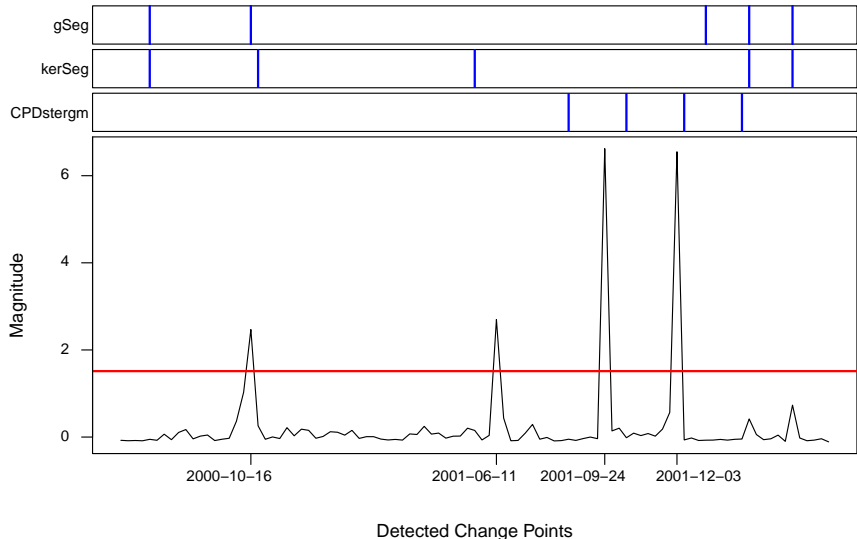


Figure 6: Detected change points from the proposed and competitor (blue) methods on the Enron email data. The threshold (red horizontal line) is calculated by (13) with $\mathcal{Z}_{0.9}$.

In 2001, Enron underwent a multitude of major incidents, making it difficult to associate the detected change points with real world events, locally. Yet, as our proposed method provides global results over the entire time frame, four crucial change points are detected for interpretation. Throughout 2000, Enron orchestrated rolling blackouts, causing staggering surges in electricity prices that peaked at twenty times the standard rate. The situation worsened when the Federal Energy Regulatory Commission (FERC) exonerated Enron of wrongdoing by the end of 2000. Subsequently, an activist physically confronted the CEO in protest against Enron’s role in the energy crisis, and Enron’s stock price plummeted after the CEO’s resignation in August 2001. Three months later, pressured by Wall Street analysts and the revelation of the scandals, Enron filed for bankruptcy and the largest energy company in the U.S. fell apart.

Table 5: Potential nearby events aligned with the detected change points from our proposed method on the Enron email data.

Detected change points	Potential nearby events
2000-10-16	2000-11-01 FERC exonerated Enron
2001-06-11	2001-06-21 CEO publicly confronted
2001-09-24	2001-08-14 CEO resigned
2001-12-03	2001-12-02 Enron filed for bankruptcy

6 Discussion

This paper proposes a generative model to detect change points in dynamic graphs. Intrinsicly, dynamic networks are complex due to dyadic and temporal dependencies. Learning low dimensional graph representations can extract useful features serving change point detection. We impose prior distributions to the graph representations, and the informative priors in the latent space are learned from data as empirical Bayes. The Group Fused Lasso problem is solved via ADMM, and the generative model is demonstrated to be helpful for change point detection.

Several extensions to our proposed framework are possible for future development. Besides binary networks, relations by nature have degree of strength, which are denoted by generic values. Moreover, nodal and dyadic attributes are important components in network data. Hence, models that generate weighted edges, as well as nodal and dyadic attributes, can capture more information about the networks (Fellows & Handcock, 2012; Krivitsky, 2012). While our framework demonstrates the ability in change point detection, the development of more sophisticated architectures can enhance the model’s capacity on other tasks and data (Handcock et al., 2007; Kolar et al., 2010; Yu et al., 2021; Madrid Padilla et al., 2023).

References

- Carlos M Alaíz, Alvaro Barbero, and José R Dorransoro. Group fused lasso. In *Artificial Neural Networks and Machine Learning–ICANN 2013: 23rd International Conference on Artificial Neural Networks Sofia, Bulgaria, September 10–13, 2013. Proceedings 23*, pp. 66–73. Springer, 2013.
- Kevin Bleakley and Jean-Philippe Vert. The group fused lasso for multiple change-point detection. *arXiv preprint arXiv:1106.4199*, 2011.
- Stephen Boyd, Neal Parikh, Eric Chu, Borja Peleato, Jonathan Eckstein, et al. Distributed optimization and statistical learning via the alternating direction method of multipliers. *Foundations and Trends® in Machine Learning*, 3(1):1–122, 2011.
- Carter T Butts. A relational event framework for social action. *Sociological Methodology*, 38(1):155–200, 2008.
- Carter T Butts, Alessandro Lomi, Tom AB Snijders, and Christoph Stadtfeld. Relational event models in network science. *Network Science*, 11(2):175–183, 2023.
- Guodong Chen, Jesús Arroyo, Avanti Athreya, Joshua Cape, Joshua T Vogelstein, Youngser Park, Chris White, Jonathan Larson, Weiwei Yang, and Carey E Priebe. Multiple network embedding for anomaly detection in time series of graphs. *arXiv preprint arXiv:2008.10055*, 2020.
- Hao Chen and Nancy Zhang. Graph-based change-point detection. *The Annals of Statistics*, 43(1):139–176, 2015.
- Lynna Chu and Hao Chen. Asymptotic distribution-free change-point detection for multivariate and non-euclidean data. *The Annals of Statistics*, 47(1):382–414, 2019.
- Jacob Devlin, Ming-Wei Chang, Kenton Lee, and Kristina Toutanova. Bert: Pre-training of deep bidirectional transformers for language understanding. *arXiv preprint arXiv:1810.04805*, 2018.
- Vijay Prakash Dwivedi, Anh Tuan Luu, Thomas Laurent, Yoshua Bengio, and Xavier Bresson. Graph neural networks with learnable structural and positional representations. *arXiv preprint arXiv:2110.07875*, 2021.
- Nathan Eagle and Alex (Sandy) Pentland. Reality mining: sensing complex social systems. *Personal and Ubiquitous Computing*, 10(4):255–268, 2006.
- Ian Fellows and Mark S. Handcock. Exponential-family random network models, 2012.
- Damien Garreau and Sylvain Arlot. Consistent change-point detection with kernels. *Electronic Journal of Statistics*, 12(2):4440 – 4486, 2018.

- Yongshun Gong, Xue Dong, Jian Zhang, and Meng Chen. Latent evolution model for change point detection in time-varying networks. *Information Sciences*, 646:119376, 2023.
- Mingqi Han, Eric A Bushong, Mayuko Segawa, Alexandre Tiard, Alex Wong, Morgan R Brady, Milica Momcilovic, Dane M Wolf, Ralph Zhang, Anton Petcherski, et al. Spatial mapping of mitochondrial networks and bioenergetics in lung cancer. *Nature*, 615(7953):712–719, 2023.
- Mark S Handcock, Adrian E Raftery, and Jeremy M Tantrum. Model-based clustering for social networks. *Journal of the Royal Statistical Society: Series A (Statistics in Society)*, 170(2):301–354, 2007.
- Steve Hanneke, Wenjie Fu, and Eric P Xing. Discrete temporal models of social networks. *Electronic Journal of Statistics*, 4:585–605, 2010.
- Xiaoxin He, Bryan Hooi, Thomas Laurent, Adam Perold, Yann LeCun, and Xavier Bresson. A generalization of vit/mlp-mixer to graphs. In *International Conference on Machine Learning*, pp. 12724–12745. PMLR, 2023.
- Jonathan Ho, Ajay Jain, and Pieter Abbeel. Denoising diffusion probabilistic models. *Advances in neural information processing systems*, 33:6840–6851, 2020.
- Shenyang Huang, Yasmeeen Hitti, Guillaume Rabusseau, and Reihaneh Rabbany. Laplacian change point detection for dynamic graphs. In *Proceedings of the 26th ACM SIGKDD International Conference on Knowledge Discovery & Data Mining*, pp. 349–358, 2020.
- Yik Lun Kei, Hangjian Li, Yanzhen Chen, and Oscar Hernan Madrid Padilla. Change point detection on a separable model for dynamic networks. *arXiv preprint arXiv:2303.17642*, 2023.
- Mladen Kolar, Le Song, Amr Ahmed, and Eric P Xing. Estimating time-varying networks. *The Annals of Applied Statistics*, pp. 94–123, 2010.
- Pavel N Krivitsky. Exponential-family random graph models for valued networks. *Electronic journal of statistics*, 6:1100, 2012.
- Pavel N Krivitsky and Mark S Handcock. A separable model for dynamic networks. *Journal of the Royal Statistical Society. Series B, Statistical Methodology*, 76(1):29, 2014.
- Federico Larroca, Paola Bermolen, Marcelo Fiori, and Gonzalo Mateos. Change point detection in weighted and directed random dot product graphs. In *2021 29th European Signal Processing Conference (EU-SIPCO)*, pp. 1810–1814. IEEE, 2021.
- Mike Lewis, Yinhan Liu, Naman Goyal, Marjan Ghazvininejad, Abdelrahman Mohamed, Omer Levy, Ves Stoyanov, and Luke Zettlemoyer. Bart: Denoising sequence-to-sequence pre-training for natural language generation, translation, and comprehension. *arXiv preprint arXiv:1910.13461*, 2019.
- Carlos Misael Madrid Padilla, Haotian Xu, Daren Wang, Oscar Hernan Madrid Padilla, and Yi Yu. Change point detection and inference in multivariable nonparametric models under mixing conditions. *arXiv preprint arXiv:2301.11491*, 2023.
- Oscar Hernan Madrid Padilla, Yi Yu, Daren Wang, and Alessandro Rinaldo. Optimal nonparametric multivariate change point detection and localization. *IEEE Transactions on Information Theory*, 68(3):1922–1944, 2021.
- Oscar Hernan Madrid Padilla, Yi Yu, and Carey E Priebe. Change point localization in dependent dynamic nonparametric random dot product graphs. *The Journal of Machine Learning Research*, 23(1):10661–10719, 2022.
- Bernardo Marenco, Paola Bermolen, Marcelo Fiori, Federico Larroca, and Gonzalo Mateos. Online change point detection for weighted and directed random dot product graphs. *IEEE Transactions on Signal and Information Processing over Networks*, 8:144–159, 2022.

- Erik Nijkamp, Mitch Hill, Tian Han, Song-Chun Zhu, and Ying Nian Wu. On the anatomy of mcmc-based maximum likelihood learning of energy-based models. In *Proceedings of the AAAI Conference on Artificial Intelligence*, volume 34, pp. 5272–5280, 2020.
- Bo Pang, Tian Han, Erik Nijkamp, Song-Chun Zhu, and Ying Nian Wu. Learning latent space energy-based prior model. *Advances in Neural Information Processing Systems*, 33:21994–22008, 2020.
- Jong Hee Park and Yunkyu Sohn. Detecting Structural Changes in Longitudinal Network Data. *Bayesian Analysis*, 15(1):133 – 157, 2020.
- Youngser Park, Carey E Priebe, and Abdou Youssef. Anomaly detection in time series of graphs using fusion of graph invariants. *IEEE journal of selected topics in signal processing*, 7(1):67–75, 2012.
- Leto Peel and Aaron Clauset. Detecting change points in the large-scale structure of evolving networks. In *Proceedings of the AAAI Conference on Artificial Intelligence*, volume 29, 2015.
- Carey E Priebe, John M Conroy, David J Marchette, and Youngser Park. Scan statistics on enron graphs. *Computational & Mathematical Organization Theory*, 11:229–247, 2005.
- Robin Rombach, Andreas Blattmann, Dominik Lorenz, Patrick Esser, and Björn Ommer. High-resolution image synthesis with latent diffusion models. In *Proceedings of the IEEE/CVF conference on computer vision and pattern recognition*, pp. 10684–10695, 2022.
- S Golshid Sharifnia and Abbas Saghaei. A statistical approach for social network change detection: an ergm based framework. *Communications in Statistics-Theory and Methods*, 51(7):2259–2280, 2022.
- Tom AB Snijders. The statistical evaluation of social network dynamics. *Sociological methodology*, 31(1): 361–395, 2001.
- Tom AB Snijders, Gerhard G Van de Bunt, and Christian EG Steglich. Introduction to stochastic actor-based models for network dynamics. *Social networks*, 32(1):44–60, 2010.
- Hoseung Song and Hao Chen. Asymptotic distribution-free changepoint detection for data with repeated observations. *Biometrika*, 109(3):783–798, 2022a.
- Hoseung Song and Hao Chen. New kernel-based change-point detection. *arXiv preprint arXiv:2206.01853*, 2022b.
- Deborah Sulem, Henry Kenlay, Mihai Cucuringu, and Xiaowen Dong. Graph similarity learning for change-point detection in dynamic networks. *Machine Learning*, pp. 1–44, 2023.
- Gerrit JJ van den Burg and Christopher KI Williams. An evaluation of change point detection algorithms. *arXiv preprint arXiv:2003.06222*, 2020.
- Jean-Philippe Vert and Kevin Bleakley. Fast detection of multiple change-points shared by many signals using group lars. *Advances in Neural Information Processing Systems*, 23, 2010.
- Jianwen Xie, Song-Chun Zhu, and Ying Nian Wu. Synthesizing dynamic patterns by spatial-temporal generative convnet. In *Proceedings of the IEEE conference on computer vision and pattern recognition*, pp. 7093–7101, 2017.
- Jianwen Xie, Yang Lu, Ruiqi Gao, Song-Chun Zhu, and Ying Nian Wu. Cooperative training of descriptor and generator networks. *IEEE transactions on pattern analysis and machine intelligence*, 42(1):27–45, 2018.
- Yi Yu, Oscar Hernan Madrid Padilla, Daren Wang, and Alessandro Rinaldo. Optimal network online change point localisation. *arXiv preprint arXiv:2101.05477*, 2021.
- Ming Yuan and Yi Lin. Model selection and estimation in regression with grouped variables. *Journal of the Royal Statistical Society Series B: Statistical Methodology*, 68(1):49–67, 2006.
- Zifeng Zhao, Li Chen, and Lizhen Lin. Change-point detection in dynamic networks via graphon estimation. *arXiv preprint arXiv:1908.01823*, 2019.

7 Appendix

7.1 Updating μ and ϕ

In this section, we derive the updates for prior parameter $\mu \in \mathbb{R}^{T \times d}$ and graph decoder parameter ϕ . Denote the objective function in Equation (4) as $\mathcal{L}(\phi, \mu)$ and denote the set of parameters $\{\phi, \mu\}$ as θ . We first calculate the gradient of the log-likelihood $l(\theta)$ in $\mathcal{L}(\phi, \mu)$ with respect to θ :

$$\begin{aligned}
\nabla_{\theta} l(\theta) &= \nabla_{\theta} \sum_{t=1}^T \log P(\mathbf{y}^t) \\
&= \sum_{t=1}^T \frac{1}{P(\mathbf{y}^t)} \nabla_{\theta} P(\mathbf{y}^t) \\
&= \sum_{t=1}^T \frac{1}{P(\mathbf{y}^t)} \nabla_{\theta} \int P(\mathbf{y}^t, \mathbf{z}^t) d\mathbf{z}^t \\
&= \sum_{t=1}^T \frac{1}{P(\mathbf{y}^t)} \int P(\mathbf{y}^t, \mathbf{z}^t) [\nabla_{\theta} \log P(\mathbf{y}^t, \mathbf{z}^t)] d\mathbf{z}^t \\
&= \sum_{t=1}^T \int \frac{P(\mathbf{y}^t, \mathbf{z}^t)}{P(\mathbf{y}^t)} [\nabla_{\theta} \log P(\mathbf{y}^t, \mathbf{z}^t)] d\mathbf{z}^t \\
&= \sum_{t=1}^T \int P(\mathbf{z}^t | \mathbf{y}^t) [\nabla_{\theta} \log P(\mathbf{y}^t, \mathbf{z}^t)] d\mathbf{z}^t \\
&= \sum_{t=1}^T \mathbb{E}_{P(\mathbf{z}^t | \mathbf{y}^t)} \left(\nabla_{\theta} \log [P(\mathbf{y}^t | \mathbf{z}^t) P(\mathbf{z}^t)] \right) \\
&= \sum_{t=1}^T \mathbb{E}_{P(\mathbf{z}^t | \mathbf{y}^t)} \left(\nabla_{\theta} \log P(\mathbf{y}^t | \mathbf{z}^t) \right) + \sum_{t=1}^T \mathbb{E}_{P(\mathbf{z}^t | \mathbf{y}^t)} \left(\nabla_{\theta} \log P(\mathbf{z}^t) \right).
\end{aligned}$$

Note that the expectation in the gradient is now with respect to the posterior distribution $P(\mathbf{z}^t | \mathbf{y}^t) \propto P(\mathbf{y}^t | \mathbf{z}^t) \times P(\mathbf{z}^t)$. Furthermore, the gradient of $\mathcal{L}(\phi, \mu)$ with respect to the prior parameter $\mu^t \in \mathbb{R}^d$ at a specific time point t is

$$\begin{aligned}
\nabla_{\mu^t} \mathcal{L}(\phi, \mu) &= -\mathbb{E}_{P(\mathbf{z}^t | \mathbf{y}^t)} \left(\nabla_{\mu^t} \log P(\mathbf{z}^t) \right) + \kappa(\mu^t - \nu^t + \mathbf{w}^t) \\
&= -\mathbb{E}_{P(\mathbf{z}^t | \mathbf{y}^t)} (\mathbf{z}^t - \mu^t) + \kappa(\mu^t - \nu^t + \mathbf{w}^t).
\end{aligned}$$

Setting the gradient $\nabla_{\mu^t} \mathcal{L}(\phi, \mu)$ to zeros and solve for μ^t , we have

$$\begin{aligned}
\mathbf{0} &= -\mathbb{E}_{P(\mathbf{z}^t | \mathbf{y}^t)} (\mathbf{z}^t) + (1 + \kappa)\mu^t - \kappa(\nu^t - \mathbf{w}^t) \\
(1 + \kappa)\mu^t &= \mathbb{E}_{P(\mathbf{z}^t | \mathbf{y}^t)} (\mathbf{z}^t) + \kappa(\nu^t - \mathbf{w}^t) \\
\mu^t &= \frac{1}{1 + \kappa} \mathbb{E}_{P(\mathbf{z}^t | \mathbf{y}^t)} (\mathbf{z}^t) + \frac{\kappa}{1 + \kappa} (\nu^t - \mathbf{w}^t).
\end{aligned}$$

Evidently, the gradient of $\mathcal{L}(\phi, \mu)$ with respect to the graph decoder parameter ϕ is

$$\nabla_{\phi} \mathcal{L}(\phi, \mu) = - \sum_{t=1}^T \mathbb{E}_{P(\mathbf{z}^t | \mathbf{y}^t)} \left(\nabla_{\phi} \log P(\mathbf{y}^t | \mathbf{z}^t) \right).$$

7.2 Langevin Dynamics

Calculating the solution in (7) and the gradient in (8) requires evaluating the conditional expectations under the posterior distribution $P(\mathbf{z}^t | \mathbf{y}^t) \propto P(\mathbf{y}^t | \mathbf{z}^t) \times P(\mathbf{z}^t)$. In this section, we discuss the Langevin Dynamics

to sample $\mathbf{z}^t \in \mathbb{R}^d$ from the posterior distribution $P(\mathbf{z}^t|\mathbf{y}^t)$ that is conditional on the observed network $\mathbf{y}^t \in \{0, 1\}^{n \times n}$. The Langevin Dynamics, a short run MCMC, is achieved by iterating the following:

$$\begin{aligned} \mathbf{z}_{\tau+1}^t &= \mathbf{z}_\tau^t + \delta[\nabla_{\mathbf{z}^t} \log P(\mathbf{z}^t|\mathbf{y}^t)] + \sqrt{2\delta}\boldsymbol{\epsilon} \\ &= \mathbf{z}_\tau^t + \delta[\nabla_{\mathbf{z}^t} \log P(\mathbf{y}^t|\mathbf{z}^t) + \nabla_{\mathbf{z}^t} \log P(\mathbf{z}^t) - \nabla_{\mathbf{z}^t} \log P(\mathbf{y}^t)] + \sqrt{2\delta}\boldsymbol{\epsilon} \\ &= \mathbf{z}_\tau^t + \delta[\nabla_{\mathbf{z}^t} \log P(\mathbf{y}^t|\mathbf{z}^t) - (\mathbf{z}_\tau^t - \boldsymbol{\mu}^t)] + \sqrt{2\delta}\boldsymbol{\epsilon} \end{aligned}$$

where τ is the time step and δ is the step size of the Langevin Dynamics. The error term $\boldsymbol{\epsilon} \sim \mathcal{N}(\mathbf{0}, \mathbf{I}_d)$ serves as a random perturbation to the sampling process. The gradient of the graph decoder $P(\mathbf{y}^t|\mathbf{z}^t)$ with respect to the latent variable \mathbf{z}^t can be calculated efficiently through back-propagation. Essentially, we use MCMC samples to approximate the conditional expectation $\mathbb{E}_{P(\mathbf{z}^t|\mathbf{y}^t)}(\cdot)$ in the solution (7) and the gradient (8).

7.3 Group Lasso for Updating β

In this section, we present the derivation to update β in Proposition 2, which is equivalent to solving a Group Lasso problem Yuan & Lin (2006). We adapt the derivation from Bleakley & Vert (2011) for our proposed ADMM algorithm. Denote the objective function in (5) as $\mathcal{L}(\gamma, \beta)$. When $\beta_{t,\cdot} \neq \mathbf{0}$, the gradient of $\mathcal{L}(\gamma, \beta)$ with respect to $\beta_{t,\cdot}$ is

$$\nabla_{\beta_{t,\cdot}} \mathcal{L}(\gamma, \beta) = \lambda \frac{\beta_{t,\cdot}}{\|\beta_{t,\cdot}\|_2} - \kappa \mathbf{X}_{\cdot,t}^\top (\boldsymbol{\mu}_{(a+1)} + \mathbf{w}_{(a)} - \mathbf{1}_{T,1}\gamma - \mathbf{X}_{\cdot,t}\beta_{t,\cdot} - \mathbf{X}_{\cdot,-t}\beta_{-t,\cdot})$$

where $\mathbf{X}_{\cdot,t} \in \mathbb{R}^{T \times 1}$ is the t -th column of matrix $\mathbf{X} \in \mathbb{R}^{T \times (T-1)}$ and $\beta_{t,\cdot} \in \mathbb{R}^{1 \times d}$ is the t -th row of matrix $\beta \in \mathbb{R}^{(T-1) \times d}$. Moreover, we denote $\beta_{-t,\cdot} \in \mathbb{R}^{(T-1) \times p}$ as the matrix obtained by replacing the t -th row of matrix β with a zero vector, and $\mathbf{X}_{\cdot,-t} \in \mathbb{R}^{T \times (T-1)}$ is denoted similarly.

Setting the above gradient to zeros, we have

$$\beta_{t,\cdot} = (\kappa \mathbf{X}_{\cdot,t}^\top \mathbf{X}_{\cdot,t} + \frac{\lambda}{\|\beta_{t,\cdot}\|_2})^{-1} \mathbf{b}_t \quad (14)$$

where

$$\mathbf{b}_t = \kappa \mathbf{X}_{\cdot,t}^\top (\boldsymbol{\mu}_{(a+1)} + \mathbf{w}_{(a)} - \mathbf{1}_{T,1}\gamma - \mathbf{X}_{\cdot,-t}\beta_{-t,\cdot}) \in \mathbb{R}^{1 \times d}.$$

Calculating the Euclidean norm of (14) on both sides and rearrange the terms, we have

$$\|\beta_{t,\cdot}\|_2 = (\kappa \mathbf{X}_{\cdot,t}^\top \mathbf{X}_{\cdot,t})^{-1} (\|\mathbf{b}_t\|_2 - \lambda).$$

Plugging $\|\beta_{t,\cdot}\|_2$ into (14) for substitution, the solution of $\beta_{t,\cdot}$ is arrived at

$$\beta_{t,\cdot} = \frac{1}{\kappa \mathbf{X}_{\cdot,t}^\top \mathbf{X}_{\cdot,t}} \left(1 - \frac{\lambda}{\|\mathbf{b}_t\|_2}\right) \mathbf{b}_t.$$

Moreover, when $\beta_{t,\cdot} = \mathbf{0}$, the subgradient \mathbf{v} of $\|\beta_{t,\cdot}\|_2$ needs to satisfy that $\|\mathbf{v}\|_2 \leq 1$. Because

$$\mathbf{0} \in \lambda \mathbf{v} - \kappa \mathbf{X}_{\cdot,t}^\top (\boldsymbol{\mu}_{(a+1)} + \mathbf{w}_{(a)} - \mathbf{1}_{T,1}\gamma - \mathbf{X}_{\cdot,-t}\beta_{-t,\cdot}),$$

we obtain the condition that $\beta_{t,\cdot}$ becomes $\mathbf{0}$ when $\|\mathbf{b}_t\|_2 \leq \lambda$. Therefore, we can iteratively apply the following to update $\beta_{t,\cdot}$ for each block $t = 1, \dots, T-1$:

$$\beta_{t,\cdot} \leftarrow \frac{1}{\kappa \mathbf{X}_{\cdot,t}^\top \mathbf{X}_{\cdot,t}} \left(1 - \frac{\lambda}{\|\mathbf{b}_t\|_2}\right)_+ \mathbf{b}_t$$

where $(\cdot)_+ = \max(\cdot, 0)$.

7.4 Practical Guidelines

7.4.1 ADMM Implementation

In this section, we provide practical guidelines for the proposed framework and the Alternating Direction Method of Multipliers (ADMM) algorithm. For Langevin Dynamic sampling, we set $\delta = 0.5$, and we draw $s = 200$ samples for each time point t . To detect change points using the data-driven threshold in (13), we let the tuning parameter $\lambda = \{10, 20, 50, 100\}$. To detect change points using the localizing method with Gamma distribution in (11), we let the tuning parameter $\lambda = \{5, 10, 20, 50\}$. For each λ , we run $A = 50$ iterations of ADMM. Within each ADMM iteration, we run $B = 20$ iterations of gradient descent with Adam optimizer for the graph decoder and $D = 20$ iterations of block coordinate descent for Group Lasso.

Since the proposed generative model is a probability distribution for the observed network data, in this work we stop ADMM learning with the following stopping criteria:

$$\left| \frac{l(\boldsymbol{\phi}_{(a+1)}, \boldsymbol{\mu}_{(a+1)}) - l(\boldsymbol{\phi}_{(a)}, \boldsymbol{\mu}_{(a)})}{l(\boldsymbol{\phi}_{(a)}, \boldsymbol{\mu}_{(a)})} \right| \leq \epsilon_{\text{tol}}. \quad (15)$$

The log-likelihood $l(\boldsymbol{\phi}, \boldsymbol{\mu})$ is approximated by sampling from the prior distribution $p(\mathbf{z}^t)$, as described in Section 4.2. Hence, we stop the ADMM procedure until the above criteria is satisfied for a' consecutive iterations. In Section 5, we set $\epsilon_{\text{tol}} = 10^{-5}$ and $a' = 5$.

Here we briefly elaborate on the computational aspect of the approximation of the log-likelihood. To calculate the product of edge probabilities for the conditional distribution $P(\mathbf{y}^t | \mathbf{z}^t)$, we have the following:

$$\begin{aligned} \sum_{t=1}^T \log P(\mathbf{y}^t) &= \sum_{t=1}^T \log \int P(\mathbf{y}^t | \mathbf{z}^t) P(\mathbf{z}^t) d\mathbf{z}^t \\ &= \sum_{t=1}^T \log \mathbb{E}_{P(\mathbf{z}^t)} \left[\prod_{(i,j) \in \mathbb{Y}} P(\mathbf{y}_{ij}^t | \mathbf{z}^t) \right] \\ &\approx \sum_{t=1}^T \log \left[\frac{1}{s} \sum_{u=1}^s \left[\prod_{(i,j) \in \mathbb{Y}} P(\mathbf{y}_{ij}^t | \mathbf{z}_u^t) \right] \right] \\ &= \sum_{t=1}^T \log \left[\frac{1}{s} \sum_{u=1}^s \exp \left\{ \sum_{(i,j) \in \mathbb{Y}} \log [P(\mathbf{y}_{ij}^t | \mathbf{z}_u^t)] \right\} \right] \\ &= \sum_{t=1}^T \left\{ -\log s + \log \left[\exp C^t \sum_{u=1}^s \exp \left\{ \sum_{(i,j) \in \mathbb{Y}} \log [P(\mathbf{y}_{ij}^t | \mathbf{z}_u^t)] - C^t \right\} \right] \right\} \\ &= \sum_{t=1}^T \left\{ C^t + \log \left[\sum_{u=1}^s \exp \left\{ \sum_{(i,j) \in \mathbb{Y}} \log [P(\mathbf{y}_{ij}^t | \mathbf{z}_u^t)] - C^t \right\} \right] \right\} - T \log s \end{aligned}$$

where $C^t \in \mathbb{R}$ is the maximum value of $\sum_{(i,j) \in \mathbb{Y}} \log [P(\mathbf{y}_{ij}^t | \mathbf{z}_u^t)]$ over m samples but within a time point t .

We also update the penalty parameter κ to improve convergence and to reduce reliance on its initialization. In particular, after the a -th ADMM iteration, we calculate the respective primal and dual residuals:

$$r_{\text{primal}}^{(a)} = \sqrt{\frac{1}{T \times d} \sum_{t=1}^T \|\boldsymbol{\mu}_{(a)}^t - \boldsymbol{\nu}_{(a)}^t\|_2^2} \quad \text{and} \quad r_{\text{dual}}^{(a)} = \sqrt{\frac{1}{T \times d} \sum_{t=1}^T \|\boldsymbol{\nu}_{(a)}^t - \boldsymbol{\nu}_{(a-1)}^t\|_2^2}.$$

Throughout, we initialize the penalty parameter $\kappa = 10$. We jointly update the penalty parameter κ and the scaled dual variable \mathbf{w} as in Boyd et al. (2011) with the following conditions:

$$\begin{aligned} \kappa_{(a+1)} &= 2\kappa_{(a)}, \quad \mathbf{w}_{(a+1)} = \frac{1}{2}\mathbf{w}_{(a)}, \quad \text{if } r_{\text{primal}}^{(a)} > 10 \times r_{\text{dual}}^{(a)}, \\ \kappa_{(a+1)} &= \frac{1}{2}\kappa_{(a)}, \quad \mathbf{w}_{(a+1)} = 2\mathbf{w}_{(a)}, \quad \text{if } r_{\text{dual}}^{(a)} > 10 \times r_{\text{primal}}^{(a)}. \end{aligned}$$

7.4.2 Post-Processing

Since neural networks may be over-fitted for a statistical model in change point detection, we track the following Coefficient of Variation as a signal-to-noise ratio when we learn the model parameter with the full data:

$$\text{Coefficient of Variation} = \frac{\text{mean}(\Delta\hat{\boldsymbol{\mu}})}{\text{sd}(\Delta\hat{\boldsymbol{\mu}})}.$$

We choose the learned parameter $\hat{\boldsymbol{\mu}}$ with the largest Coefficient of Variation as final output.

By convention, we also implement two post-processing steps to finalize the detected change points. When the gap between two consecutive change points is small or $\hat{C}_k - \hat{C}_{k-1} < \epsilon_{\text{spc}}$, we preserve the detected change point with greater $\Delta\hat{\boldsymbol{\zeta}}$ value to prevent clusters of nearby change points. Moreover, as the endpoints of a time span are usually not of interest, we remove the \hat{C}_k smaller than a threshold ϵ_{end} and the \hat{C}_k greater than $T - \epsilon_{\text{end}}$. In Section 5, we set $\epsilon_{\text{spc}} = 5$ and $\epsilon_{\text{end}} = 5$.